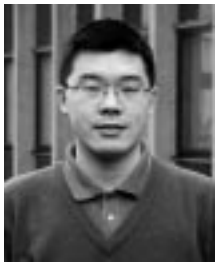

Journal of Thermal Analysis and Calorimetry, Vol. 64 (2001) 85–107

TEMPERATURE MODULATED DIFFERENTIAL SCANNING CALORIMETRY
Part IV. Effect of heat transfer on the measurement of heat capacity using quasi-isothermal ADSC

Z. Jiang[1]*, C. T. Imrie*[1] *and J. M. Hutchinson*[2*]

[1]Department of Chemistry, University of Aberdeen, Aberdeen AB24 3UE, United Kingdom
[2]Department of Engineering, University of Aberdeen, Aberdeen AB24 3UE, United Kingdom

Abstract

An analysis developed in previous work has been further refined in order to study the effect of heat transfer on the heat capacity and phase angle measurements by TMDSC. In the present model, a temperature gradient within the sample has been taken into account by allowing for heat transfer by thermal conduction within the sample. The influence of the properties of the sensors, the heat transfer conditions between the sensor and sample, and the properties of the sample have been investigated by varying each parameter in turn. The results show that heat capacity measurements are reliable only within a restricted frequency range, for which the experimental conditions are such that the heat transfer phase angle depends linearly on the modulation frequency.

Keywords: complex heat capacity, heat transfer, phase angle, TMDSC

Introduction

It is widely recognised that one of the main advantages of TMDSC is its ability to measure the heat capacity and the change in heat capacity of a sample under isothermal conditions by calculating the ratio of the amplitude of the modulated heat flow to the amplitude of the modulated heating rate [1–5]. However, it has also been noted that the measured heat capacity deviates from the literature value and becomes increasingly inaccurate as the frequency increases [6–8]. The difference between the measured and literature values depends on the experimental conditions and the properties of the sample. For instance, the measured heat capacity of sapphire under quasi-isothermal conditions is in good agreement with the literature value over a relatively wide range of modulation periods (from 30 to 90 s with an amplitude of 0.2 K) for a small sample mass (about 10 mg). For sample masses up to 50 mg, and for a pe-

* Author to whom all correspondence should be addressed.

1418–2874/2001/ $ 5.00
Akadémiai Kiadó, Budapest

riod of 60 s and amplitude of 0.2 K, it remains constant, but then falls by more than 10% when the sample mass increases to 100 mg [1]. In contrast, for polymers the measured heat capacity is relatively constant for a sample mass of several milligrams only when measured with periods such as 60 s, or even longer than 120 s for some polymers [7, 8]. These observations have been attributed, at least qualitatively, to the effect of heat transfer between the DSC and sample, and to the fact that for a relative short period a temperature gradient builds up within the sample because of the problem of thermal conduction [1, 2, 9–11].

Due to the lack of a systematic analysis of heat transfer within the TMDSC system, however, this hypothesis has not been fully tested. Indeed, the data in the literature are rather contradictory. A typical example is the investigation of the relationship between the measured heat capacity and the modulation frequency for different materials. Cser *et al.* [7] observed that the heat capacity of sapphire measured using frequencies in the range from 0.01 to 0.10 rad s^{-1} (periods between approximately 600 and 60 s) decreased as a function of the square of the frequency, whereas the heat capacity of high density polyethylene decreased linearly with increasing frequency.

Our view is that the measured heat capacity can remain constant only when the phase angle depends linearly on the modulation frequency, as suggested by our previous work on the effect of heat transfer on the phase angle [11]. These heat transfer effects were considered, however, with the assumption that the temperature of the sample is uniform throughout its thickness. More realistically, though, the influence of the temperature gradient in the sample on the TMDSC measurement, particularly for short periods (high frequencies), should not be neglected. In the present work, the effect of heat transfer on the heat capacity measurement will be discussed in terms of the contributions arising from the properties of the sensor, the heat transfer interface between sensor and sample, and the properties of the sample, within the framework of a further refinement of our previous model to allow for thermal conduction within the sample itself. Using this model, it is also possible to analyse the heat transfer in a multi-layer system of either homogeneous or heterogeneous materials.

Theory of heat capacity measurement by TMDSC

In this section we review briefly the assumptions inherent in and the conclusions drawn from an earlier simpler model of TMDSC, identified schematically by Model B in Fig. 1. The temperatures on the sample side and reference side of the TMDSC cell are considered to be measured experimentally by sensors, as indicated, with the properties of the sample side and reference side sensors being identical. This implies that in the absence of any sample there will be no measured temperature difference between sample and reference side, and hence no heat flow; in practice there will usually be some asymmetry in the construction of the TMDSC cell, and hence a certain heat flow even with no sample, but this can be allowed for by an appropriate calibration procedure.

In the present and earlier models, it is assumed that it is the reference side sensor that follows exactly the programmed temperature, consisting of a sinusoidal modula-

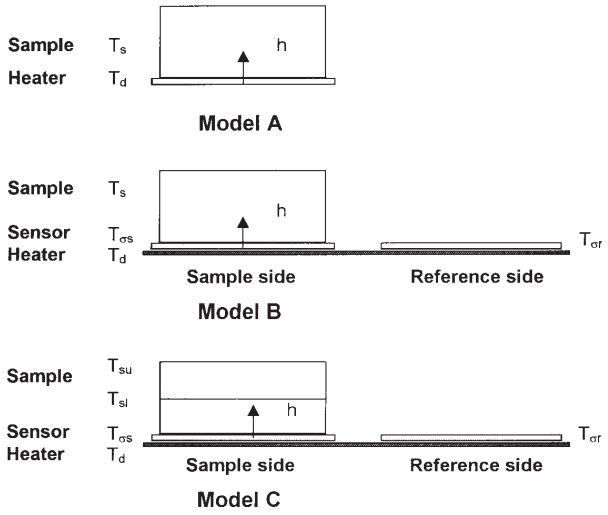

Fig. 1 The present heat transfer model (Model C) and earlier models (A and B) for comparison

tion superimposed in general on a linear heating (or cooling) rate, as expressed by Eq. (1) below. This corresponds, of course, to a sinusoidally modulated heating rate and gives rise to the modulated heat flow as the output, from which the heat capacity can be determined. In the analysis that follows, the symbols used throughout are listed for the convenience of the reader at the end of the text and before the Appendix.

The measured specific heat capacity is calculated from the ratio of the heat flow to the heating rate, and may make use of the average values (for $C_{p,ave}$, which is analogous to the specific heat capacity obtained by conventional DSC) or the amplitudes (for the complex specific heat capacity, C_p^*). The heat flow is found from the temperature difference ΔT between the reference ($T_{\sigma r}$) and sample ($T_{\sigma s}$) sensors, the temperatures of which are shown later to be:

$$T_{\sigma r} = T_0 + \beta_0 t + A_T \sin\omega t \tag{1}$$

$$T_{\sigma s} = T_0 + \beta_0 (t - P_s) + A_{\sigma s} \sin(\omega t + \phi_{\sigma s}) \tag{2}$$

where T_0 is the initial temperature, t is time, β_0 is the underlying heating rate, A_T is the amplitude of temperature modulation, $A_{\sigma s}$ is the amplitude of sample side sensor temperature modulation, ω is the frequency of the temperature modulation, $\phi_{\sigma s}$ is the phase difference between reference and sample side sensor temperatures, and P_s is a parameter equivalent to a time constant and defined as:

$$P_s = \frac{m_s C_{p,s} L_\sigma}{k_\sigma Y} \tag{3}$$

where m_s and $C_{p,s}$ are the mass and specific heat capacity of the sample, respectively, L_σ and k_σ are the thickness and thermal conductivity of the sensor, respectively, and Y is the contact area between sensor and sample.

Therefore:

$$\Delta T = T_{\sigma r} - T_{\sigma s} = \beta_0 P_s + A_T \sin\omega t - A_{\sigma s} \sin(\omega t + \phi_{\sigma s}) \quad (4)$$

and the instantaneous heating rate β can be written as:

$$\beta = \dot{T}_{\sigma r} = \beta_0 + A_T \omega \cos(\omega t) \quad (5)$$

Now, the heat capacity can be defined as either an average value or a complex value, as follows.

i) Specific average heat capacity, $C_{p,ave}$.

The specific average heat capacity, $C_{p,ave}$, may be calculated from the ratios of the average values of the specific heat flow, q m_s^{-1}, and the heating rate, β, as follows:

$$C_{p,ave} = \frac{\bar{q}}{m_s \bar{\beta}} \propto \frac{\overline{\Delta T}}{\bar{\beta}} = \frac{\beta_0 P_s}{\beta_0} = P_s \quad (6)$$

where the superscript bars indicate average values.

It can be seen that $C_{p,ave}$ returns the input value for the specific heat capacity of the sample, $C_{p,s}$, and is independent of the modulation frequency. However, it cannot be measured under quasi-isothermal conditions because the average heating rate is zero, and the specific average heat capacity has no meaning under these conditions.

ii) Specific complex heat capacity, C_p^*.

According to Schawe's definition [12], the modulus of the specific complex heat capacity $|C_p^*|$ is written as:

$$\left|C_p^*\right| = \left|\frac{A_q}{m_s A_\beta}\right| = \text{constant} \frac{A_{\Delta T}}{A_\beta} \quad (7)$$

where A_q and A_β are the amplitudes of the heat flow and heating rate, respectively, and $A_{\Delta T}$ is the amplitude of the temperature difference ΔT. This latter may be derived from the expression for ΔT given by Eq. (4), which gives:

$$A_{\Delta T} = \sqrt{A_{\sigma s}^2 \phi_{\sigma s}^2 + (A_T - A_{\sigma s})^2} \quad (8)$$

for quasi-isothermal experiments for which $\beta_0 = 0$, while A_β is obtained from Eq. (5) as:

$$A_\beta = A_T \omega \quad (9)$$

Clearly the specific complex heat capacity can be defined even under quasi-isothermal conditions. However, it can be seen that the complex heat capacity measurement is greatly influenced by $A_{\sigma s}$ and $\phi_{\sigma s}$, in other words by the effect of heat transfer and by the modulation frequency. These effects were discussed in our earlier work [10, 11], and are considered again in more detail here.

Model of heat transfer in TMDSC under quasi-isothermal conditions

Two previous heat transfer models for TMDSC are illustrated schematically in Fig. 1 and denoted as Model A and Model B. Model A was suggested by Wunderlich and co-workers [1, 2], in which the measured temperature was assumed to be the sample temperature, T_s, and the heat transfer from heater to sample is influenced by the heat transfer coefficient, h. In this model, the phase angle between sample and heater temperatures was examined. In Model B, the measured temperature is regarded as the sensor temperature [11], and hence the TMDSC measurement is not only affected by heat transfer between the sample and sensor but also by the thermal properties of the sensor. However, in Model B, it is assumed for simplicity that thermal conduction within the sample is infinitely large. This is a reasonable approximation only for thin or highly thermally conductive materials, and at low frequency, which implies that, under most situations, heat transfer within the sample itself should be considered. Therefore, a further refinement (Model C) is examined in this work in which the sample is divided into two layers, and heat transfer between the two layers occurs by thermal conduction.

The mathematical approach adopted here, and in our earlier work also [10, 11], is very similar to that used by Ozawa and Kanari [4, 13], though there are significant differences in detail. These authors, for example, include heat loss to the surroundings as well as mutual heat exchange between the sample and reference sides, whereas these effects are not included in the present analysis. There are also differences in that Ozawa and Kanari select the sample temperature as the reference modulation, with the measured output signal being the temperature difference between sample and reference, whereas we select the reference sensor for the programmed modulation, with the temperature difference between the sample side and reference side sensors providing the measured output signal. Clearly the sample itself will have a different amplitude and phase from those of the sample side sensor, which was in part the subject of our earlier work [11]. These differences will be seen to be even more pronounced in the present work where the finite thermal conductivity of the sample implies a temperature gradient in the sample, and hence the impossibility of defining a unique sample temperature.

It should also be pointed out that Model C remains highly simplified. The sensors respond to the heat input from the TMDSC heater (or furnace), with heat transfer occurring by conduction through highly conductive materials, even if the geometry of the cell is considerably more complex than is implied by the schematic diagram. Also, the sample will usually be contained in an aluminium pan, with a corresponding pan on the reference side; these have been omitted in order to simplify the analysis, but could be included in an exactly analogous way in a more detailed model. Likewise, heat loss from both sample and reference sides is ignored, but could be modelled by the inclusion of a heat transfer coefficient from sample and reference to the surroundings.

As mentioned above, the reference side sensor temperature is assumed to follow the programmed temperature (Eq. (1)). In an analogous way to the derivation of Eq. (2), the heater temperature T_d can be expressed in the steady state as:

$$T_d = T_0 + \beta_0 (t + P_\sigma) + A_d \sin(\omega t + \phi_d) \tag{10}$$

in which P_σ is a time constant for the sensor, and is given by (see also Appendix, Eq. (A17)):

$$P_\sigma = \frac{m_\sigma C_{p,\sigma} L_\sigma}{k_\sigma Y} \tag{11}$$

and A_d and ϕ_d can be expressed as $A_d = A_T \sqrt{1+\omega^2 P_\sigma^2}$ and $\phi_d = \arctan(\omega P_\sigma)$. Here, m_σ and $C_{p,\sigma}$ are the mass and specific heat capacity of the sensor, and the analysis is based on the assumption that the heat flow by conduction from heater to the sensor is proportional, by a factor $m_\sigma C_{p\sigma}$, to the rate of change of sensor temperature, assuming no heat loss.

On the sample side, the heat flow from heater to sensor is:

$$q_{d\to\sigma s} = k_\sigma Y (T_d - T_{\sigma s})/L_\sigma \tag{12}$$

while that from the sensor to the lower sample layer is, as before:

$$q_{\sigma s\to sl} = hY (T_{\sigma s} - T_{sl}) \tag{13}$$

and that from the lower sample layer to the upper sample layer is:

$$q_{sl\to su} = k_s Y (T_{sl} - T_{su})/L_s \tag{14}$$

The subscripts sl and su refer to the lower and upper sample layers, respectively. Furthermore, we can write:

$$q_{d\to\sigma s} - q_{\sigma s\to sl} = m_\sigma C_{p,\sigma} \dot{T}_{\sigma s} \tag{15}$$

$$q_{\sigma s\to sl} - q_{sl\to su} = m_{sl} C_{p,sl} \dot{T}_{sl} \tag{16}$$

and

$$q_{sl\to su} = m_{su} C_{p,su} \dot{T}_{su} \tag{17}$$

again assuming no heat loss to the surroundings. In order to proceed, the temperatures of the sample side sensor, lower sample layer and upper sample layer may be written in general as:

$$T_{\sigma s} = a_1 + b_1 t + c_1 e^{-t/\tau_1} + d_1 \sin\omega t + e_1 \cos\omega t \tag{18}$$

$$T_{sl} = a_2 + b_2 t + c_2 e^{-t/\tau_2} + d_2 \sin\omega t + e_2 \cos\omega t \tag{19}$$

$$T_{su} = a_3 + b_3 t + c_3 e^{-t/\tau_3} + d_3 \sin\omega t + e_3 \cos\omega t \tag{20}$$

The derivatives with respect to time of Eqs (18)–(20), can be expressed as:

$$\dot{T}_{\sigma s}=b_1-\frac{c_1}{\tau_1}\mathrm{e}^{-t/\tau_1}+d_1\omega\cos\omega t-e_1\omega\sin\omega t \tag{21}$$

$$\dot{T}_{sl}=b_2-\frac{c_2}{\tau_2}\mathrm{e}^{-t/\tau_2}+d_2\omega\cos\omega t-e_2\omega\sin\omega t \tag{22}$$

$$\dot{T}_{su}=b_3-\frac{c_3}{\tau_3}\mathrm{e}^{-t/\tau_3}+d_3\omega\cos\omega t-e_3\omega\sin\omega t \tag{23}$$

If we consider the steady state condition, then the terms including c_1, c_2 and c_3 are zero and the net heat flow into the sample side sensor can be related to its rate of change of temperature by Eq. (15), which becomes:

$$k_\sigma Y(T_d-T_{\sigma s})/L_\sigma-hY(T_{\sigma s}-T_{sl})=m_\sigma C_{p,\sigma}\dot{T}_{\sigma s} \tag{24}$$

where $\dot{T}_{\sigma s}$ is given by Eq. (21) and the other temperatures by Eqs (10), (18) and (19). Likewise, the net heat flow into the sample at the lower layer can be written from Eqs (13), (14), and (16) as:

$$hY(T_{\sigma s}-T_{sl})-k_{su}Y(T_{sl}-T_{su})/L_{su}=m_{sl}C_{p,sl}\dot{T}_{sl} \tag{25}$$

and from the heat transfer into the insulated upper layer of the sample we can write, from Eqs (14) and (17):

$$k_{su}Y(T_{sl}-T_{su})/L_{su}=m_{su}C_{p,su}\dot{T}_{su} \tag{26}$$

The solution to this heat transfer problem is given in the Appendix, and can conveniently be expressed in matrix form as:

$$\begin{bmatrix} 1 & 0 & 0 & -\omega P_\sigma & -\omega P_{s,sl} & -\omega P_{s,su} \\ -1 & 1 & 0 & 0 & -\omega P_{h,sl} & -\omega P_{h,su} \\ 0 & -1 & 1 & 0 & 0 & -\omega S_{su} \\ \omega P_\sigma & \omega P_{s,sl} & \omega P_{s,su} & 1 & 0 & 0 \\ 0 & \omega P_{h,sl} & \omega P_{h,su} & -1 & 1 & 0 \\ 0 & 0 & \omega S_{su} & 0 & -1 & 1 \end{bmatrix}\begin{bmatrix} d_1 \\ d_2 \\ d_3 \\ e_1 \\ e_2 \\ e_3 \end{bmatrix}=\begin{bmatrix} 1 \\ 0 \\ 0 \\ \omega P_\sigma \\ 0 \\ 0 \end{bmatrix}A_T \tag{27}$$

where P_σ, $P_{s,sl}$, $P_{s,su}$, $P_{h,sl}$, $P_{h,su}$ and S_{su} are time constants given by Eqs (A17) to (A22), respectively.

The matrix above applies to any sample which consists of two layers, and which may in general be different. If we now consider the special case in which each layer is identical, thus allowing simply for thermal conduction within a uniform and homogeneous sample, then $m_{sl}=m_{su}=m_s/2$ where m_s is the total sample mass, and we can further simplify these equations by writing $P_s=2P_{s,sl}=2P_{s,su}$, $P_h=2P_{h,sl}=2P_{h,su}$, and $S=S_{su}$.

Assuming steady state conditions, we can thus write the sample side sensor temperature as:

$$T_{\sigma s}=T_0+\beta_0(t-P_s)+A_{\sigma s}\sin(\omega t+\phi_{\sigma s}) \quad (2)$$

where P_s is given by Eq. (3), $A_{\sigma s}=\sqrt{d_1^2+e_1^2}$ and $\phi_{\sigma s}$ is the phase angle between sample sensor temperature and reference sensor temperature given by:

$$\phi_{\sigma s}=\arctan\left(\frac{e_1}{d_1}\right) \quad (28)$$

or, by replacing e_1 and d_1 with expressions obtained from the matrix Eq. (27):

$$\phi_{\sigma s}=\arctan(e_1/d_1)$$

$$\text{where } e_1=-\omega P_s[4-2\omega^2(P_\sigma P_h+P_\sigma S-S^2)-\omega^4 P_\sigma P_h S^2] \text{ and} \quad (29a)$$

$$d_1=4+2\omega^2(2P_\sigma^2+2P_sP_\sigma+2P_sP_h+2P_h^2+P_sS+2P_hS+2S^2)+$$

$$+\omega^4(P_h^2S^2+4P_\sigma P_h^2+4P_\sigma^2P_hS+4P_h^2S^2+2P_sP_\sigma S^2+P_sP_hS^2)+\omega^6(P_\sigma^2P_h^2S^2) \quad (29b)$$

Likewise, the lower sample temperature may be written:

$$T_{sl}=T_0+\beta_0[t-(P_s+P_h)]+A_{sl}\sin(\omega t+\phi_{sl}) \quad (30)$$

where $A_{sl}=\sqrt{d_2^2+e_2^2}$ and ϕ_{sl} is the phase angle between the temperature of the lower sample layer and the reference sensor temperature, and is given by:

$$\phi_{sl}=\arctan\left(\frac{e_2}{d_2}\right) \quad (31)$$

The upper sample temperature may be written as:

$$T_{su}=T_0+\beta_0[t-(P_s+P_h)-S]+A_{su}\sin(\omega t+\phi_{su}) \quad (32)$$

where $A_{su}=\sqrt{d_3^2+e_3^2}$ and ϕ_{su} is the phase angle between the temperature of the upper sample layer and the reference sensor temperature:

$$\phi_{su}=\arctan\left(\frac{e_3}{d_3}\right) \quad (33)$$

In the limit of low frequencies, these phase angles become:

$$\lim_{\omega\to0}\phi_{\sigma s}\to-\omega(P_s) \quad (34)$$

$$\lim_{\omega\to0}\phi_{sl}\to-\omega(P_s+P_h) \quad (35)$$

$$\lim_{\omega\to0}\phi_{su}\to-\omega(P_s+P_h+S) \quad (36)$$

From Eq. (34), it can be seen that, for small phase angles, the phase angle of the sample sensor depends linearly on frequency and is again proportional to sample mass, sample specific heat capacity and sensor properties (Eqs (A18) and (A19)). Meanwhile, if the heat transfer from sensor to sample is infinitely fast ($h\to\infty$), then $P_h\to0$ (Eq. (A20)), the temperature of the sample side sensor is identical to that of the lower layer of the sample, and Eq. (35) can be rewritten as:

$$\underset{\omega\to 0}{\phi_{sl}} \to -\omega P_s = -\omega \frac{2m_{sl}C_{p,sl}L_\sigma}{k_\sigma Y} \tag{37}$$

which is identical to the analogous equation derived from Model A [1, 2]. It should be noted, however, that this identity occurs only in the limit $\omega\to 0$. There are two reasons for this restriction.

First, despite the fact that Eq. (37) is derived assuming infinitely good heat transfer to the lower sample layer, there still remains the upper sample layer with heat transfer by conduction to it from the lower sample layer. This is only eliminated if the thermal conductivity is infinite, in which case $S\to 0$, and from Eq. (36) we obtain an equation identical to Eq. (37) for the upper sample layer.

The restriction $\omega\to 0$ still applies in respect of a comparison with Model A, however, for the second reason. This is that in Model A the phase angle is considered between the sample temperature and the heater temperature, whereas here the phase angle is between the sensors on the sample and reference sides. For this reason, in our model with $h\to\infty$ and $k\to\infty$ there remains a non-linear dependence of phase angle $\phi_{\sigma s}$ on frequency, which can be shown from the matrix Eq. (27) with $P_h=0$ and $S=0$ to be given by:

$$\phi_{\sigma s} = \arctan\left[\frac{-\omega P_s}{1+\omega^2 P_\sigma (P_\sigma + P_s)}\right] \tag{38}$$

From this it is clear that for optimum conditions we require a small value for P_σ, the time constant for the sensor.

To examine the effect of finite values of h and k on the measured specific complex heat capacity, we must return to Eqs (7)–(9), from which the modulus of the specific complex heat capacity can be written:

$$\left|C_p^*\right| = \text{constant}\frac{1}{\omega}\sqrt{\left(1-\frac{A_{\sigma s}}{A_T}\right)^2 + \left(\frac{A_{\sigma s}}{A_T}\right)^2 \phi_{\sigma s}^2} \tag{39}$$

The general expression with $A_{\sigma s}=\sqrt{d_1^2+e_1^2}$ and $\phi_{\sigma s}$ given by Eqs (28) and (29) is too complex to derive any simple frequency dependence for $|C_p^*|$. It is clear, though, that at sufficiently low frequency that $A_{\sigma s}\approx A_T$, the dependence in Eq. (39) reduces to $\phi_{\sigma s}/\omega$ which, from Eq. (34), leads to a constant, frequency independent, value for the complex specific heat capacity. In general, however, $A_{\sigma s}<A_T$ and $-\phi_{\sigma s}<\omega P_s$, and these inequalities increase with increasing frequency such that $|C_p^*|$ deviates increasingly from its zero frequency value. The magnitude of this deviation depends on the heat transfer conditions and on the properties of the sample, in particular, and its evaluation requires numerical analysis. Nevertheless, it is clear that significant deviation of C_p^* from its correct value generally occurs when the phase angle departs from a linear frequency dependence, and further comment on this is made in the sections that follow.

In this work, we investigate the effect of heat transfer from the sensor to the bottom layer of the sample, and also of that from the bottom to the top layer within the sample, on the dependence of both the phase angle and the specific complex heat capacity on the modulation frequency. These theoretical predictions are then compared with the experimentally measured values of C_p^* for polycarbonate under quasi-isothermal conditions.

Experimental

Materials

Polycarbonate was used for the TMDSC measurements of complex specific heat capacity and phase angle as a function of modulation frequency. It has a glass transition temperature of approximately 145°C. The extrusion grade polycarbonate (Lexan, GE Plastics), was obtained as a solid rod 40 mm diameter (trade name Tecanat) extruded by Ensinger, from which the samples were machined. Smaller rods, with diameter 5 mm to suit the aluminium crucibles (pans) of the DSC, were turned and then parted on a lathe into discs of thickness ranging from 0.25 to 1.50 mm.

Quasi-isothermal ADSC programs

The particular variant of TMDSC used here was Alternating DSC (ADSC, Mettler-Toledo). Quasi-isothermal ADSC experiments were performed at a constant temperature of 100°C, in other words in the glassy state for polycarbonate, with a modulated temperature amplitude of 0.5 K; the period was varied between 30 and 1200 s. The intracooler was used for all measurements and nitrogen was used as the purge gas with a flow rate of 80 ml min^{-1}.

Simulations

The theoretical simulations based on Model C essentially require the solution of the matrix Eq. (27) for selected values of the parameters defining the simulated conditions. These calculations have been performed using MATLAB (version 4.2, Copyright © 1984–1994 by The Mathworks, Inc.). The main parameters used in the simulation are: k_σ=0.6 W m^{-1} K^{-1}, L_σ=1 mm, Y=19.6 mm^2, m_σ=30 mg, $C_{p,\sigma}$=0.5 J g^{-1} K^{-1}, m_s=12.0 mg, k_s=0.2 W m^{-1} K^{-1}, and $C_{p,s}$=1.5 J g^{-1} K^{-1}, unless otherwise specified.

Results and discussion

The theoretical predictions for the effects of the instrumental parameters on the phase angle and on the specific heat capacity measurement have been simulated in terms of three aspects, namely the properties of the sensor, the heat transfer coefficient at the interface between the sensor and sample, and the properties of the sample.

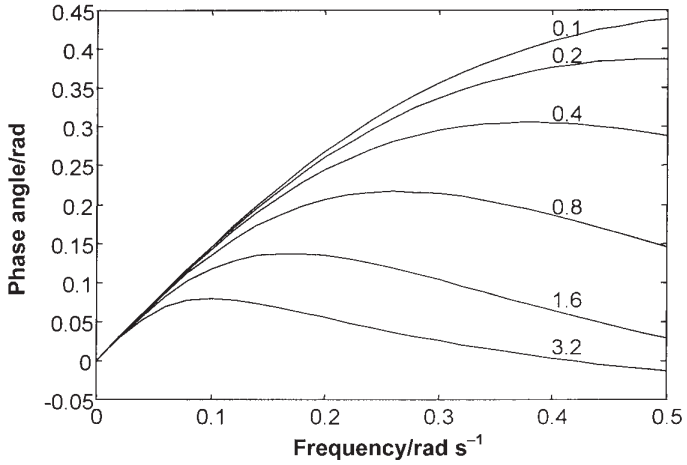

Fig. 2 The effect of $C_{p,\sigma}$ on the (negative) phase angle, $\phi_{\sigma s}$. (k_σ=0.6 W m^{-1} K^{-1}; L=0.5 mm; h=2000 W m^{-2} K^{-1}). The value of $C_{p,\sigma}$ is indicated in units of J g^{-1} K^{-1} *vs*. each curve

Effect of the sensor properties

It has been shown that the influence of the sensor on the TMDSC measurement is described by the parameters P_σ and P_s (Eqs (A17), (A18) and (A19)). Indeed, this is true even under idealised conditions for which the heat transfer coefficient from sensor to sample and the thermal conductivity of the sample are both infinite, as shown by Eq. (38). These observations mean that the effect of heat transfer is related not only to k_σ but also to the density, the specific heat capacity, and the geometric size of the sensor. However, because of the complexity of the design of a real sensor, the analysis has been simplified in this work by considering the density and dimensions of the sensor to be fixed while the specific heat capacity and thermal conductivity have been varied.

The effect of the specific heat capacity of the sensor is shown in Fig. 2: as the specific heat capacity of the sensor increases, $-\phi$ decreases and its maximum value appears at a lower frequency, while all the curves for the various values of $C_{p,\sigma}$ converge to a linear region at low frequency, all having the same slope, P_s (Eqs (3) and (34)). From the analysis of Model C, changing the specific heat capacity of the sensor only changes P_σ (refer to Eq. (A17)). Since the numerator in Eq. (29) indicates that the departure from linearity with increasing frequency is determined principally by the term $P_\sigma P_h + P_\sigma S - S^2$, it follows that this departure from linearity will occur at a lower frequency as P_σ, and hence the specific heat capacity of the sensor, increases, as is seen in Fig. 2.

Figure 3 illustrates the influence of the specific heat capacity of the sensor, $C_{p\sigma,}$, on the measurement of C_p^* for the sample. When $C_{p,\sigma}$ decreases from 3.20 to 0.10 J g^{-1} K^{-1}, the upper limit of the measuring frequency for an error of 2% in the specific heat capacity of the sample increases from 0.026 to 0.24 rad s^{-1} (a period

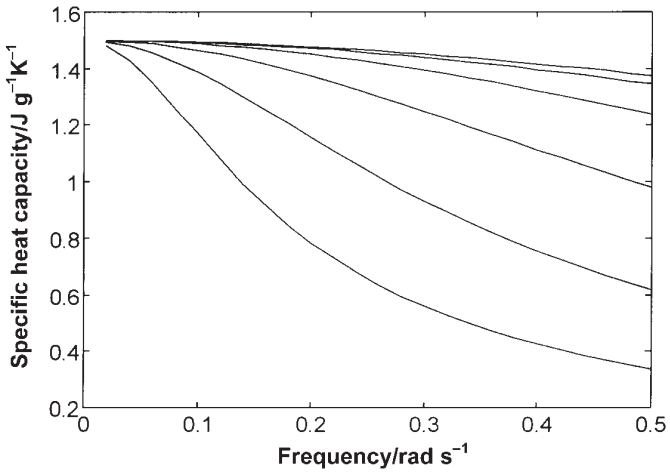

Fig. 3 The effect of $C_{p,\sigma}$ on the measured C_p^* for frequencies from 0.02 to 0.50 rad s^{-1}. Values of $C_{p,\sigma}$ are taken as 0.1 (top), 0.2, 0.4, 0.8, 1.6 and 3.2 (bottom) J g^{-1} K^{-1}. Values of k_σ, L and h are the same as for Fig. 2

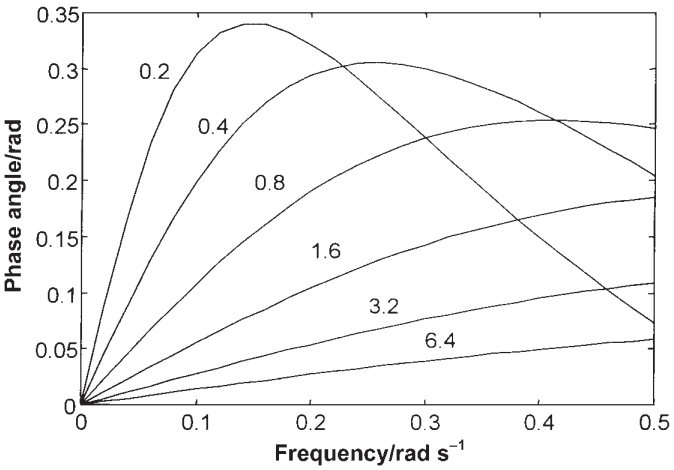

Fig. 4 The effect of k_σ on the (negative) phase angle $\phi_{\sigma s}$. ($C_{p,\sigma}$=0.5 J g^{-1} K^{-1}; L=0.5 mm; h=2000 W m^{-2} K^{-1}). The value of k_σ is indicated in units of W m^{-1} K^{-1} *vs.* each curve

range of approximately 240 to 24 s). With regard to the measurement of C_p^*, therefore, sensors with small heat capacities can enlarge the frequency range over which acceptable measurements can be made. The small $C_{p,\sigma}$, however, will cause an increase of the phase angle (refer to Fig. 2).

The corresponding effect of the thermal conductivity of the sensor on the phase angle measurements is shown in Fig. 4, from which two points should be noted. On

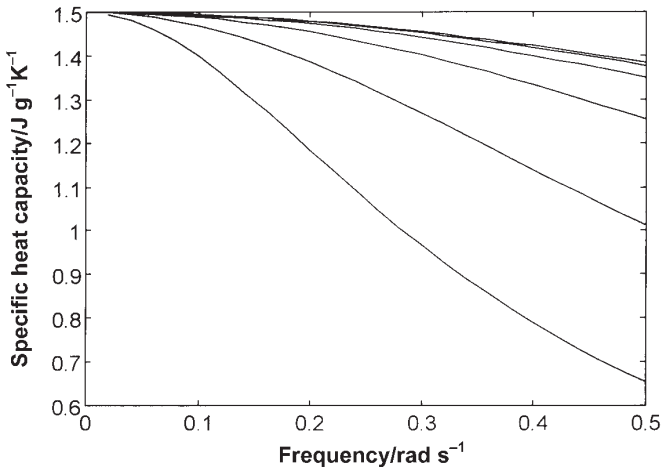

Fig. 5 The effect of k_σ on the measured C_p^* over a range of frequencies from 0.02 to 0.50 rad s^{-1}. The values of k_σ are 0.2 (bottom), 0.4, 0.8, 1.6, 3.2 and 6.4 (top) W m^{-1} K^{-1}. Values of $C_{p,\sigma}$, L and h are the same as for Fig. 4

the one hand, $-\phi$ for the sensor with different values of k_σ again increases linearly at low frequency, but with differing slopes as P_s is proportional to $1/k_\sigma$ (refer to Eqs (3), (A18) and (A19)). On the other hand, with increasing k_σ the maximum $-\phi$ appears at higher frequencies because in the numerator of Eq. (29) the terms $2\omega^2(P_\sigma P_h+P_\sigma S-S^2)$ and $\omega^4 P_\sigma P_h S^2$ decrease as k_σ increases, as a result of the decrease in P_σ (Eq. (A17)). In consequence, the region for which a linear dependence of the phase angle on frequency is observed extends to higher frequencies as k_σ increases.

Figure 5 explores the effect of the thermal conductivity of the sensors on the measured complex specific heat capacity, C_p^*. Under the conditions adopted, the measured C_p^* value decreases with increasing frequency, in a manner that is dependent upon the thermal conductivity of the sensors k_σ (it was assumed here that the sample and reference sensors have identical properties). When k_σ is 0.2 W m^{-1} K^{-1}, the value of C_p^* drops from 1.50 to 0.65 J g^{-1} K^{-1}, which corresponds to a reduction of over 50% over the frequency range of 0 to 0.5 rad s^{-1}. In the most widely used period range of 90~30 s (frequency of 0.07~0.21 rad s^{-1}), the measured value of C_p^* is up to 25% less than the true value. On the other hand, when k_σ takes the largest value, 6.4 W m^{-1} K^{-1}, the decrease in C_p^* over the whole range is less than 15%. If the acceptable error is ±2% (however, in the simulation, the positive error is impossible), the measuring frequency used should not exceed 0.24 rad s^{-1} (periods down to 26 s) for k_σ=6.4 W m^{-1} K^{-1}. Referring back to Fig. 4, for k_σ=0.2 W m^{-1} K^{-1} the phase angle measured at 0.07 rad s^{-1} has already deviated from linearity; in contrast, for k_σ=6.4 W m^{-1} K^{-1} the phase angle at a frequency of 0.24 rad s^{-1} is still linearly related to the frequency. Thus, it is clear that k_σ can greatly affect the measurement of C_p^* and that, compared with the contribution of $C_{p,\sigma}$ to the TMDSC measurement, increasing

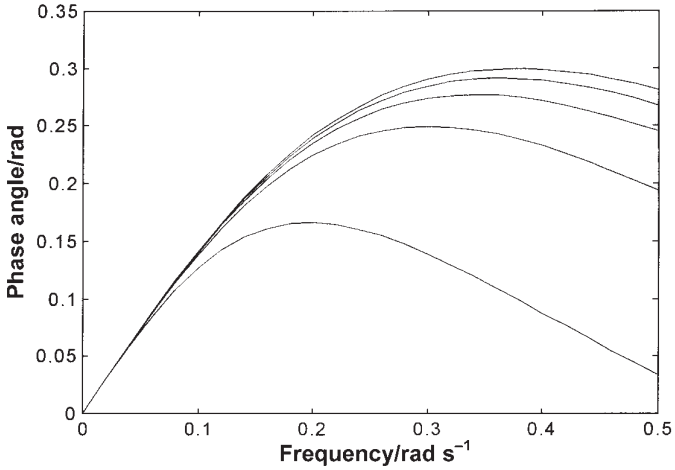

Fig. 6 Simulation of the effect of heat transfer coefficient h on the (negative) phase angle, $\phi_{\sigma s}$; h increases linearly from 400 (bottom) to 3600 W m^{-2} K^{-1} (top) with an interval of 800 W m^{-2} K^{-1}

k_σ not only expands the measuring frequency range, but also decreases the phase angle by means of reducing the effect of heat transfer in the sensor.

Effect of heat transfer conditions

Figure 6 shows the relationship between the phase angle and modulation frequency for different values of the heat transfer coefficient, h, from which it can be seen that at low frequencies $-\phi$ depends linearly on the frequency with a gradient of P_s. The linear regime is from 0 to 0.05 rad s^{-1} for poor heat transfer from the sensor to sample, for example, h=400 W m^{-2} K^{-1}, and reaches up to just less than 0.10 rad s^{-1} for good heat transfer (h=3600 W m^{-2} K^{-1}). In fact, the phase angle appears to increase rapidly when h increases from 400 to 1200 W m^{-2} K^{-1}, and then remains rather constant when h is increased further. This means that the contribution of thermal conduction within the sample to the overall resistance to heat flow first increases and then stabilises as the interface resistance decreases. The factors which cause the deviation of the frequency dependence of the phase angle from linearity can be identified by an examination of the various terms in Eq. (29), from which it is clear that this deviation depends not only on the heat transfer from sensor to sample, but also on the properties of the sensor and sample.

The quality of the heat transfer interface between the sensor and sample has a significant effect on the measured specific heat capacity, as is illustrated in Fig. 7. Increasing h can reduce the effect of frequency on the measured specific heat capacity, similar to expanding the range of linearity between $\phi_{\sigma s}$ and ω (refer to Fig. 6); however, both Figs 6 and 7 show that the effect becomes very small when h reaches values of 1200 W m^{-2} K^{-1} and larger. Therefore, although polishing the sample surface or

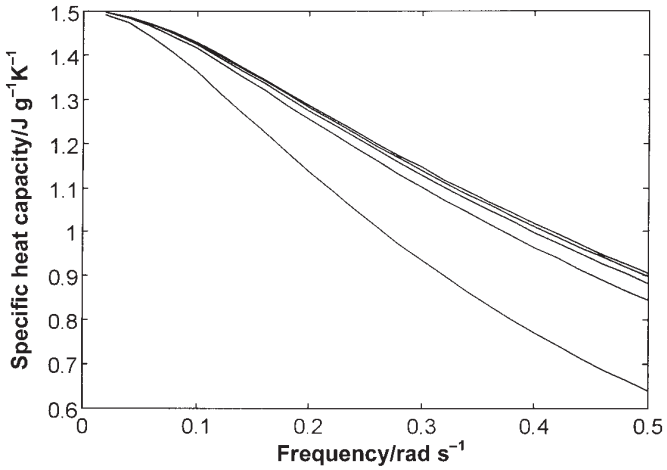

Fig. 7 The effect of heat transfer coefficient h on the measured complex specific heat capacity over a frequency range from 0.02 to 0.50 rad s^{-1}. The heat transfer coefficient, h, increases linearly from 400 (bottom) to 3600 W m^{-2} K^{-1} (top) with an interval of 800 W m^{-2} K^{-1}

introducing a heat transfer fluid is helpful in ensuring more consistent heat transfer conditions, they have little use in expanding the modulation frequency range for C_p^* measurement.

Effect of sample properties

We turn now to the effect of the properties of the sample, such as sample thickness and thermal conductivity, on the deviation of the measured C_p^* value from the real value.

Figure 8 shows how the phase angle depends on the sample thickness for Model C. As a comparison, the results calculated from Model B [11] are also shown in the figure (dashed lines). At low frequency, the phase angle for samples with different thicknesses is linearly dependent on the frequency, and the curves for samples of the same thickness converge to the same slope for Models B and C. This slope is given by P_s in Eq. (3), from which it can be seen to increase linearly with sample mass m_s, and hence also with sample thickness L_s. Increasing the sample thickness in both models narrows the frequency range in which a linear relationship between the phase angle and frequency is observed.

Indeed, the departure from linearity is particularly marked here, and this can be understood from a consideration of Eq. (29). Changing the sample thickness, and hence sample mass, has an effect on both P_h and S (Eqs (A20), (A21) and (A22)), and both of these parameters contribute to the non-linear terms in the numerator of Eq. (29), thus accentuating the effect of the sample thickness. One can also see from Fig. 8 that $-\phi$ from Model C (full lines) is significantly smaller than that obtained using Model B (dashed lines), and that this is true in general as a function of frequency

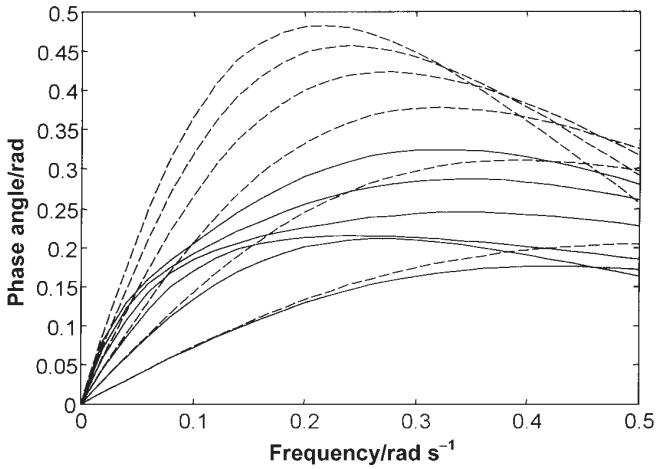

Fig. 8 The effect of sample thickness on the (negative) phase angle $\phi_{\sigma s}$. Thickness ranges linearly from 0.25 (bottom) to 1.50 mm (top) with an interval of 0.25 mm. (h=2000 W m^{-2} K^{-1}; k=0.6 W m^{-1} K^{-1}; $C_{p,\sigma}$=0.5 J g^{-1} K^{-1}). Solid lines are for Model C and dashed lines for Model B

and particularly at lower frequency for thick samples, though a cross-over does occur eventually as the frequency increases. This implies, as noted earlier, that increased resistance to heat transfer, in this case from a finite thermal conductivity, reduces the phase angle.

According to Model B, the maximum value of $-\phi$ shifts to higher frequency and decreases monotonically with decreasing sample thickness. In contrast, the predictions from Model C show that the dependence on sample thickness of the maximum value of $-\phi$, and of the frequency at which it occurs, is more complex. The maximum value of $-\phi$ increases as the sample thickness is increased from 0.25 to 1.50 mm. At the same time, it shifts to lower frequencies when the thickness increases from 0.25 to 0.75 mm, but shifts back to higher frequencies for thicknesses of 1.00, 1.25 and 1.50 mm. Further discussion of the effect of sample thickness on the frequency dependence of the phase angle in the light of the prediction from Eq. (29) is rather difficult on account of the complexity of the expression in the denominator of this equation.

Figure 9 shows that the measured C_p^* decreases with increasing frequency. The decrease over the simulation frequency range increases from 16 to 36% when the sample thickness increases from 0.1 to 0.6 mm. This means that the acceptable measuring frequency range for which the decrease in the measured C_p^* is less than 2% of the original value is considerably narrowed as the sample thickness increases. This is in good agreement with experimental specific heat capacity measurements on polycarbonate using TMDSC, shown in Fig. 10, from which it can be seen that the measured C_p^* for polycarbonate depends on both the modulation frequency and the sample thickness. With decreasing frequency, C_p^* at 100°C tends to a constant value of 1.62 J g^{-1} K^{-1}, which is very close to the value (1.63 J g^{-1} K^{-1}) measured by conventional DSC with a heating rate of 20°C min^{-1}. It is clear from both the simulation and

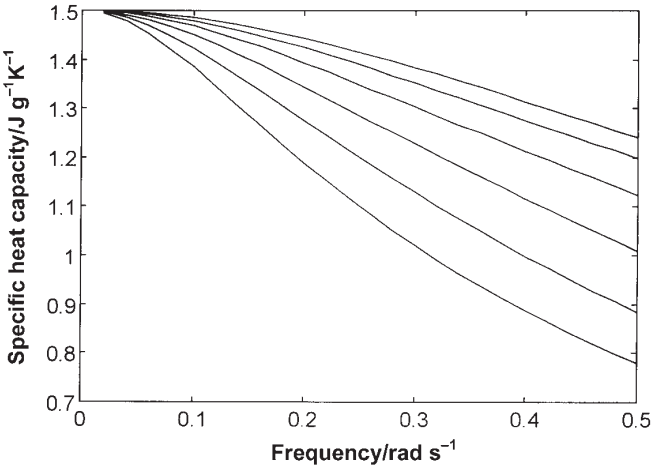

Fig. 9 The effect of sample thickness on the measured specific heat capacity. Thickness ranges between 0.1 (top) and 0.6 mm (bottom) with an interval of 0.1 mm. Values of h, k_σ and $C_{p,\sigma}$ are the same as for Fig. 8

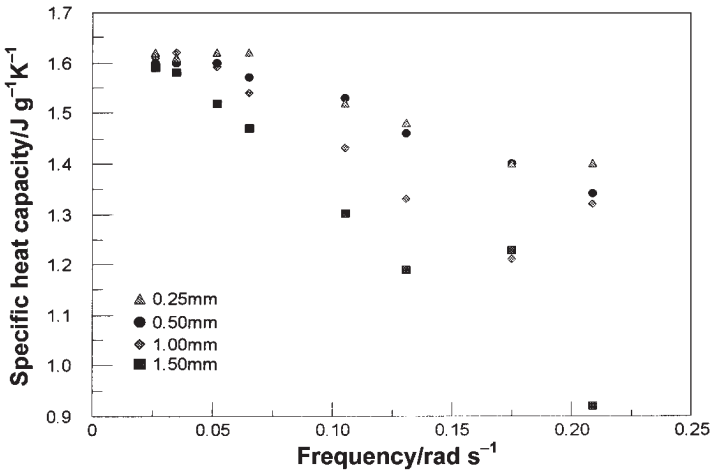

Fig. 10 The measured specific heat capacity of polycarbonate at 100°C by TMDSC. The modulation periods used are 30, 36, 48, 60, 96, 120, 180 and 240 s. The corresponding frequencies are 0.209, 0.175, 0.131, 0.105, 0.065, 0.052, 0.035 and 0.026 rad s^{-1}, respectively

the experimental results that if a thinner sample is used, a constant value of C_p^* is achieved up to a higher frequency. In Fig. 10, the experimentally measured effect of sample thickness is not as regular as that predicted in the simulation (Fig. 9). This is partly attributed to the different surface qualities for different samples, which may cause a variation of the heat transfer coefficient. Another source may be introduced by the different heat losses from the side walls of the samples with different thick-

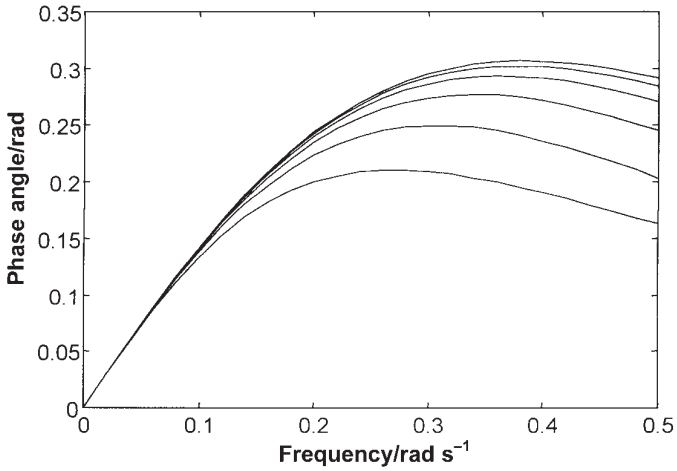

Fig. 11 The effect of k_s on the (negative) phase angle $\phi_{\sigma s}$. Values of k_s are 0.05, 0.1, 0.2, 0.4, 0.8 and 1.6 W m^{-1} K^{-1} in order from bottom to top (h=2000 W m^{-2} K^{-1}; k_σ=0.6 W m^{-1}K^{-1}; $C_{p,\sigma}$=0.5 J g^{-1}K^{-1})

nesses, which has not been taken into account in Model C. Also, the experimental results at frequencies of 0.17 and 0.21 rad s^{-1} (36 and 30 s of periods, respectively) are not very reliable, particularly for the samples with larger masses, since at these frequencies the maximum heating or cooling rate is outside the limits of the ADSC, and is also affected by the Taulag of instrument, with the consequence that the temperature modulation is deformed slightly from the ideal sinusoidal wave. Thus the measured specific heat capacity values for these two frequencies should be treated with some caution.

Figure 11 shows the effect of the sample thermal conductivity, k_s, on the phase angle. With increasing k_s the phase angle becomes larger, and the region over which there is a linear relationship between the phase angle and frequency is extended. For example, given the conditions used to construct Fig. 11, the frequency dependence of the phase angle can be regarded as linear over a range from 0 to approximately 0.06 rad s^{-1} for k_s=0.1 W m^{-1} K^{-1} which is a typical value for the thermal conductivity of a polymer; for k_s=1.6 W m^{-1} K^{-1}, the upper limit of the frequency for linearity is extended to about 0.08 rad s^{-1}. This corresponds to a change in the period of modulation, from 104.7 to 78.5 s. It is thus apparent that the linearity between the phase angle and frequency extends over a wider frequency range for high conductivity materials than for low conductivity materials.

The results also show that the effect on the phase angle caused by changing the thermal conductivity of the sample diminishes significantly as k_s increases, and that the difference between the phase angle for different values of k_s can be observed more easily at high frequency than at low frequency. This point is very important because it implies a lack of sensitivity of the phase angle to the thermal conductivity of the sam-

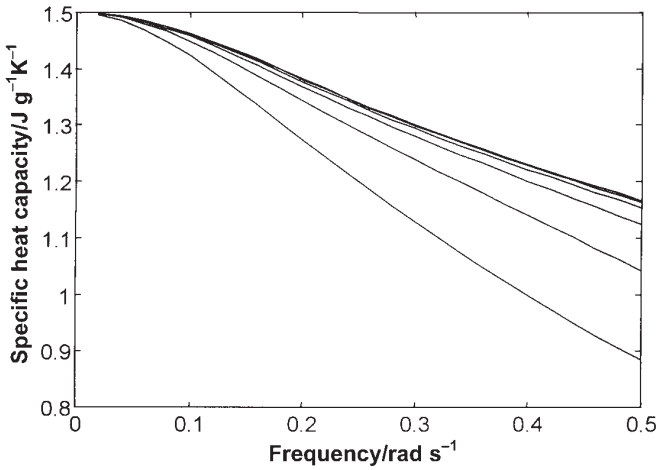

Fig. 12 The effect of k_s on the measured specific heat capacity for frequencies from 0.02 to 0.50 rad s^{-1}. Values of k_s are 0.05 (bottom), 0.10, 0.20, 0.40, 0.80 and 1.60 (top) W m^{-1} K^{-1}. Values of h, k_σ and $C_{p,\sigma}$ are the same as for Fig. 11

ple within certain ranges of frequency and k_s. For instance, suppose that a series of samples, with thermal conductivities from 0.05 to 1.6 W m^{-1} K^{-1}, are used to simulate the results shown in Fig. 11. If an experiment is performed at a frequency of 0.1 rad s^{-1}, the response of the phase angle in TMDSC shows only about a 5% difference between the phase angle corresponding to the lowest and highest values of the thermal conductivity. On the other hand, if the experiment is performed at 0.3 rad s^{-1}, the difference in the phase angle is increased to 40%. Likewise, at a frequency of 0.2 rad s^{-1} (period approximately 30 s), for example, there is a much more significant change in the phase angle for the lower thermal conductivities than for the higher thermal conductivities. This would imply that the phase angle is sensitive to changes in the thermal conductivity of poor thermal conductors, including polymers for which typical values fall in the range 0.1 to 0.3 W m^{-1} K^{-1}, but is rather insensitive to changes in the thermal conductivity of better thermal conductors.

The effect of the thermal conductivity of the sample, k_s, on the C_p^* measurements is shown in Fig. 12. As the modulation frequency increases, the measured C_p^* drops much more rapidly for a sample with a lower k_s value than it does for a sample with higher k_s value. In practice, therefore, the modulation period used for a lower k_s sample should be much longer than that for a higher k_s sample. This is one reason why the C_p^* value for a 10 mg sample of sapphire (k_s=2.6 W m^{-1} K^{-1} and C_p=0.91 J g^{-1} K^{-1} at 373 K) can be measured with a period of 30 s [1], whilst for a 5 mg polystyrene sample (k_s=0.128 W m^{-1} K^{-1}, C_p=1.62 J g^{-1} K^{-1} at 373 K) the period was suggested to be longer than 120 s [8].

The effects of the properties of the sample on the measured C_p^* determine the basis of choosing reliable modulation conditions for the measurements. In general, a thin and dense sample having a smooth contact surface with the crucible should be measured with a relatively long period of the temperature modulation, and this is par-

ticularly important for poor thermally conducting materials. The commonly used range of the period for a polymer with a mass of 5 mg (k_s ranging 0.1~0.3 W m^{-1} K^{-1}) is 60~240 s.

Conclusions

A more realistic model (Model C) than either of those used in earlier work (Model A or Model B) has been developed to study the effect of heat transfer on the phase angle and heat capacity measurements by TMDSC. In this latest model, a temperature gradient within the sample has been taken into account by allowing for heat transfer by thermal conduction within the sample. The influence of the DSC sensors, the heat transfer conditions between the sensor and sample, and the properties of the sample have been investigated by varying each parameter in turn. The effect of the sample thickness on the measurement was also studied experimentally. The results show that increasing the thermal conductivity of the sensor effectively enlarges the measuring range of modulation frequency over which an accurate value of heat capacity can be measured by quasi-isothermal TMDSC. Decreasing the heat capacity of the sensor also expands the useful modulation frequency range, although it results in a larger phase lag between the heat flow and heating rate. An improved heat transfer interface between sample and sensor will help to measure heat capacity more precisely. The effects of the thickness and the thermal conductivity of the sample on the C_p^* measurement show that tests with a thinner sample provide better results than with a thicker sample. For thicker samples, a relatively long period is needed. The results from the simulation also show that a wider frequency range can be applied in measurements of samples with higher thermal conductivity. In general, it is concluded that reliable values for C_p^* may be obtained when the experimental conditions are such that the heat transfer phase angle depends linearly on the modulation frequency. When a significant departure of the phase angle from a linear dependence on frequency occurs, this is a sure sign that the measured specific complex heat capacity will decrease significantly below its correct value if the frequency of modulation is further increased. Thus, the measurement of the phase angle can provide a check on the validity of the measured value of C_p^*.

List of symbols

A – amplitude
C_p – specific heat capacity
h – heat transfer coefficient
k – thermal conductivity
L – thickness
m – mass
P – parameter with dimensions of time (Eqs (A17–A21))
q – heat flow

S – parameter with dimensions of time (Eq. (A22))
t – time
T – temperature
Y – contact area
β – heating rate
ϕ – phase angle
ω – angular frequency

List of subscripts

d – DSC heater
h – heat transfer coefficient
q – heat flow
s – sample
sl – lower sample layer
su – upper sample layer
T – temperature
β – heating rate
ΔT – temperature difference
σ – sensor
σr – reference side sensor
σs – sample side sensor

Appendix

Solution of heat transfer equations

Substituting Eqs (10) and (18) to (23) into Eqs (24) to (26), and equating coefficients, gives the following:

i) Constant coefficients

$$k_\sigma Y(T_0+\beta_0 P_\sigma - a_1)/L_\sigma - hY(a_1-a_2)=m_\sigma C_{p,\sigma} b_1 \quad \text{(A1)}$$

$$hY(a_1-a_2)-k_{su}Y(a_2-a_3)/L_{su}=m_{sl}C_{p,sl}b_2 \quad \text{(A2)}$$

$$k_{su}Y(a_2-a_3)/L_{su}=m_{su}C_{p,su}b_3 \quad \text{(A3)}$$

ii) Coefficients of t

$$k_\sigma Y(\beta_0-b_1)/L_\sigma - hY(b_1-b_2)=0 \quad \text{(A4)}$$

$$hY(b_1-b_2)-k_{su}Y(b_2-b_3)/L_{su}=0 \quad \text{(A5)}$$

$$k_{su}Y(b_2-b_3)/L_{su}=0 \quad \text{(A6)}$$

iii) Coefficients of sinωt

$$k_\sigma Y(A_T - d_1)/L_\sigma - hY(d_1 - d_2) = m_\sigma C_{p,\sigma}(-e_1\omega) \quad \text{(A7)}$$

$$hY(d_1 - d_2) - k_{su} Y(d_2 - d_3)/L_{su} = m_{sl} C_{p,sl}(-e_2\omega) \quad \text{(A8)}$$

$$k_{su} Y(d_2 - d_3)/L_{su} = m_{su} C_{p,su}(-e_3\omega) \quad \text{(A9)}$$

iv) Coefficients of cosωt

$$k_\sigma Y(\omega P_\sigma A_T - e_1)/L_\sigma - hY(e_1 - e_2) = m_\sigma C_{p,\sigma}(d_1\omega) \quad \text{(A10)}$$

$$hY(e_1 - e_2) - k_{su} Y(e_2 - e_3)/L_{su} = m_{sl} C_{p,sl}(d_2\omega) \quad \text{(A11)}$$

$$k_{su} Y(e_2 - e_3)/L_{su} = m_{su} C_{p,su}(d_3\omega) \quad \text{(A12)}$$

From Eqs (A4), (A5) and (A6), one finds:

$$b_1 = b_2 = b_3 = \beta_0 \quad \text{(A13)}$$

and hence from Eqs (A1), (A2) and (A3), the constants a_1, a_2 and a_3 may be obtained as:

$$a_1 = T_0 - \beta_0 (P_{s,sl} + P_{s,su}) = T_0 - \beta_0 P_s \quad \text{(A14)}$$

$$a_2 = T_0 - \beta_0 \lfloor (P_{s,sl} + P_{s,su}) + (P_{h,sl} + P_{h,su}) \rfloor = T_0 - \beta_0 (P_s + P_h) \quad \text{(A15)}$$

$$a_3 = T_0 - \beta_0 \lfloor (P_{s,sl} + P_{s,su}) + (P_{h,sl} + P_{h,su}) + S_{su3} \rfloor = T_0 - \beta_0 (P_s + P_h + S) \quad \text{(A16)}$$

where:

$$P_\sigma = \frac{m_\sigma C_{p,\sigma} L_\sigma}{k_\sigma Y} \quad \text{(A17)}$$

$$P_{s,sl} = \frac{m_{sl} C_{p,sl} L_\sigma}{k_\sigma Y} \quad \text{(A18)}$$

$$P_{s,su} = \frac{m_{su} C_{p,su} L_\sigma}{k_\sigma Y} \quad \text{(A19)}$$

$$P_{h,sl} = \frac{m_{sl} C_{p,sl}}{hY} \quad \text{(A20)}$$

$$P_{h,su} = \frac{m_{su} C_{p,su}}{hY} \quad \text{(A21)}$$

$$S_{su} = \frac{m_{su} C_{p,su} L_{su}}{k_{su} Y} \quad \text{(A22)}$$

References

1 A. Boller, Y. Jin and B. Wunderlich, J. Thermal Anal., 42 (1994) 307.
2 B. Wunderlich, Y. Jin and A. Boller, Thermochim. Acta, 238 (1994) 277.
3 M. Pyda, A. Boller, J. Grebowicz, H. Chuah, B. V. Lebedev and B. Wunderlich, J. Polym. Sci.: Part B: Polym. Phys., 36 (1998) 2499.
4 T. Ozawa and K. Kanari, J. Therm. Anal. Cal., 54 (1998) 521.
5 G. Van Assche, A. Van Hemelrijck, H. Rahier and B. Van Mele, Thermochim. Acta, 268 (1995) 121.
6 J. Cao, Y. Long and R. A. Shanks, J. Thermal Anal., 50 (1997) 365.
7 F. Cser, F. Rasoul and E. Kosior, J. Thermal Anal., 50 (1997) 727.
8 B. Schenker and F. Stager, Thermochim. Acta, 304/305 (1997) 219.
9 J. E. K. Schawe and W. Winter, Thermochim. Acta, 298 (1997) 9.
10 Z. Jiang, C. T. Imrie and J. M. Hutchinson, Thermochim. Acta, 315 (1998) 1.
11 Z. Jiang, C. T. Imrie and J. M. Hutchinson, Thermochim. Acta, 336 (1999) 27.
12 J. E. K. Schawe, Thermochim. Acta, 261 (1995) 183.
13 T. Ozawa and K. Kanari, Thermochim. Acta, 288 (1996) 39.